# Metal-inorganic-organic core–shell material as efficient matrices for CO2 adsorption: Synthesis, properties and kinetic studies

Julien Vieillard, Nabil Bouazizi, Radhouane Bargougui, P. Nkuigue Fotsing, O. Thoumire, G. Ladam, Nicolas Brun, J.-F. Hochepied, E. Djoufac Woumfo, Nadine Mofaddel, et al.

# Metal-inorganic-organic core–shell material as efficient matrices for CO2 adsorption: Synthesis, properties and kinetic studies

Article In, J. Vieillard, N. Bouazizi, R. Bargougui, P. Nkuigue Fotsing, O. Thoumire, G. Ladam, N. Brun, J.-F. Hochepied, E. Djoufac Woumfo, et al.

# Metal-inorganic-organic core–shell material as efficient matrices for $CO_2$ adsorption: Synthesis, properties and kinetic studies

J. Vieillard[a,*], N. Bouazizi[a], R. Bargougui[a], P. Nkuigue Fotsing[b], O. Thoumire[c], G. Ladam[c], N. Brun[d], J.-F. Hochepied[e,f], E. Djoufac Woumfo[b], N. Mofaddel[a], F. Le Derf[a], A. Azzouz[g,*]

[a] Normandie Université, COBRA, UMR 6014 and FR3038, Université de Rouen, INSA Rouen, CNRS, 55, rue saint germain, 27000 Evreux, France
[b] Laboratoire de Physico-Chimie des Matériaux Minéraux, Département de Chimie Inorganique, Faculté des Sciences, Université de Yaoundé I, B.P. 812 Yaoundé, Cameroon
[c] Normandie Université, PBS 6270, Université de Rouen, CNRS, Centre Universitaire d'Evreux, 1 rue du 7ème chasseur, 27002 Evreux Cedex, France
[d] Institut Charles Gerhardt, ENSCM, 34296 Montpellier Cedex 5, France
[e] MINES Paris Tech, PSL Research University, Centre for Materials Studies, BP 87, 91003 Evry, France
[f] ENSTA Paris Tech, Paris-Saclay University, Unité Chimie et Procédés, 828 bd des Maréchaux, 91762 Palaiseau Cedex, France
[g] Nanoqam, Department of Chemistry, University of Quebec at Montreal, QC H3C 3P8, Canada

ARTICLE INFO

*Article history:*
Received 2 May 2018
Revised 16 July 2018
Accepted 10 August 2018
Available online xxx

*Keywords:*
Hydrochar
Cocoa shell
Copper impregnation
Core–shell
$CO_2$ adsorption
Hydrothermal treatment

ABSTRACT

A novel hydrochar-based core–shell material with improved affinity towards $CO_2$ was synthesized through encapsulation within ZnO shell, followed by chemical grafting to an organic moiety bearing terminal diethanolamino groups and further dispersion of $Cu^0$ nanoparticles. Characterization through nitrogen adsorption–desorption isotherms with BET and BJH models, SEM, TEM, zeta potential measurements, FTIR spectroscopy, DSC and XPS analyses revealed a strong influence of the modification procedure on the performance of each material in $CO_2$ adsorption. The resulting metal-inorganic-organic-core–shell (MIOCS) displayed compacted structure with a wide pore size distribution that imposes intraparticle diffusion as a kinetic-controlling step. Cu-MIOCS showed an appreciable $CO_2$ retention capacity of 5.42 mmol/g compared to many adsorbents reported so far. This affinity towards $CO_2$ was explained in terms of physical and non-stoichiometric $CO_2$ condensation. This finding is of great importance, because it demonstrates that judicious modifications of vegetal-deriving wastes such as woods and other biomasses give rise to added-value materials as low cost and efficient gas adsorbents with high affinity towards $CO_2$.

## 1. Introduction

Global warming and climate changes turn out to arise from high concentrations of greenhouse gases (GHG), among which carbon dioxide ($CO_2$) is the most directly related to human activities [1,2]. The persistent use of fossil fuels as the main energy source in designing new technologies clearly demonstrates the lack of a clear strategy for a sustainable development. This makes that GHG and $CO_2$ emissions from anthropic activities still remain a major environmental issue [3,4]. Clear evidence in this regard is provided by numerous procedures targeting direct $CO_2$ capture from flue emissions [5,6,7], even if, in most cases, adsorbents regeneration often requires more $CO_2$-equivalent energy than captured. Amine-based adsorbents display sufficient basicity for retain $CO_2$ via the formation of carbamates [8,9], but severe thermal regeneration. In the long run, this way of acting is doomed to failure, unless strategies regarding $CO_2$ as a product, for instance, for further uses in chemistry and in agricultural greenhouses are developed. Such strategies will certainly face a major issue, that of the too low $CO_2$ concentrations in flue emissions, which impose previous concentration of the captured gas.

A judicious approach in this direction resides in designing new waste-free and non-polluting technologies for $CO_2$ concentration through a truly reversible gas capture at ambient conditions. Weaker $CO_2$–adsorbent interactions are an essential requirement in this regard, and can be achieved using materials bearing amphoteric to slightly basic chemical functions such as hydroxyl groups. The latter are known to promote only $CO_2$ adsorption via weakly bonded carbonate-like association [10–17].

OH-enriched materials containing soya-deriving polyglycerols were already found to show high affinity towards $CO_2$, and gave

* Corresponding authors at: Normandie Université, COBRA, UMR 6014 and FR3038, Université de Rouen, INSA Rouen, CNRS, 55, rue saint germain, 27000 Evreux, France; Nanoqam, Department of Chemistry, University of Quebec at Montreal, QC H3C 3P8, Canada.
*E-mail addresses:* julien.vieillard@univ-rouen.fr (J. Vieillard), azzouz.a@uqam.ca (A. Azzouz).

Please cite this article as: J. Vieillard et al., Metal-inorganic-organic core–shell material as efficient matrices for $CO_2$ adsorption: Synthesis, properties and kinetic studies, Journal of the Taiwan Institute of Chemical Engineers (2018), https://doi.org/10.1016/j.jtice.2018.08.020

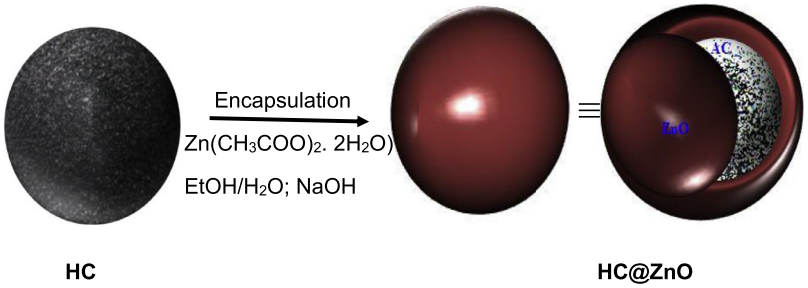


**Scheme 1.** Schematic illustration of HC@ZnO core–shell particles.

similar performances as polyol dendrimers [11,12,13,14,15,16,17]. Their affinity improvement was explained in terms of mere incorporation of a vegetal source of OH groups. Unlike complex structure materials such as zeolites, metal-organic frameworks (MOFs) and others tested in $CO_2$ adsorption [18,19,20], low cost natural materials such as vegetal wastes display low surface acidity and do not require sophisticated modification procedures [21,22]. The structure of any vegetal material should bear terminal hydroxyl groups but does not necessarily exhibit interesting affinity towards $CO_2$ due to structure constraints such as porosity and/or optimum amphoteric to slightly character.

Vegetal waste modification often turns out to an essential requirement for affinity improvement. Their conversion into hydrochar (HC), followed by suitable modifications could be a judicious route for obtaining highly added-value materials with improved affinity towards $CO_2$. HCs are also low cost porous materials that display high porosity and specific surface area along with appreciable thermal and chemical stability [23,24]. They may be obtained through pyrolysis, carbonization or hydrothermal conversion of diverse vegetal wastes [25,26]. Their activation in optimal conditions is known to improve the surface properties [27] and affinity towards $CO_2$ [28].

So far, the behavior of vegetal wastes as host matrices for metal, metal oxides and $CO_2$ condensation along with the interactions involved still remains barely tackled. This became the main objective of the present paper. Metal oxides, and more particularly zinc oxide (ZnO) are also assumed to exhibit interesting surface properties as adsorbent [29,30] and electronic material [31]. ZnO combination with a diethanolamine-modified cocoa shell-deriving hydrochar already showed interesting surface properties [32–35]. It turned out to act as host matrice for copper-zero dispersion and as effective adsorbent for $CO_2$ at room temperature like other materials with attenuated basicity [15]. The specific surface area was not an essential requirement, inasmuch as compacted matrices paradoxically displayed higher affinity towards $CO_2$ than much more expanded and more porous materials [14,36,37]. Hence, a new strategy was rather focused on the preparation of compacted matrices that promote metal stabilization and attenuate $CO_2$ retention strength. Strong metal: matrice interaction is expected to attenuate the Lewis basicity of the N atom of the organic moiety [35], and, subsequently, $CO_2$ capture will mainly occur via purely physical gas condensation, that favors with easy release upon forced convection or under lower pressure. The material interactions with both metal particles and $CO_2$ were deeply examined herein as specific objectives of this work.

Due to their low thermal and chemical stability, vegetal-deriving materials cannot be directly used in $CO_2$ capture from flue emissions. Previous cooling and water treatments of flue emissions with energy recovery with advanced elimination of $SO_x$, $NO_x$ and volatile organic compounds (VOC) turns out to be essential requirements for a possible sustainable technology. That is why reversible capture of $CO_2$ appears as an original alternative for a non-thermal gas release for regeneration and further $CO_2$ utilization. This new concept still remains a difficult challenge, but can be addressed using metal-inorganic-organic core–shell materials (MIOCS) displaying weak basicity. In this regard, our approach resides in correlating $Cu^0$-matrice and $CO_2$-matrice interactions with both the surface properties and structural and textural features of the synthesized material. Full characterization of MIOCS by means of diverse techniques allowed achieving deep analysis of the adsorbent affinity towards $CO_2$ in terms of magnitude and adsorption kinetics. The results will open promising prospects for manufacturing adsorbing materials and membranes that "respire $CO_2$" under ambient conditions.

## 2. Experimental

### 2.1. Chemicals

Zinc acetate dihydrate ($Zn(CH_3COO)_2{,}2H_2O$; 99%); 3-chloropropyltrimethoxysilane ($C_6H_{15}ClO_3Si$; 97%); sodium borohydride ($NaBH_4$; 99%); diethanolamine ($NH(CH_2–CH_2–OH)_2$; 98%); copper(II) sulfate anhydrous ($CuSO_4$; 99.9%); triethylamine ($C_6H_{15}N$; 99.9%) and absolute ethanol ($CH_3CH_2OH$; 99.9%) were purchased from Sigma-Aldrich and used as received. For all the experiments, ultra-pure water was used (Millipore).

### 2.2. Materials synthesis

Hydrochar (HC) was produced via hydrothermal conversion of cocoa shell powder (1 g), originating from Cameroon, previously dispersed in deionized water (10 mL), at 240 °C for 24 h in a sealed Teflon lined autoclave (30 mL). The mixture was cooled down to room temperature (RT), and HC was obtained in the form of a white suspension. HC was filtered, repeatedly washed with deionized water and then with ethanol, and finally dried at 80 °C overnight.

HC was then encapsulated into a shell of ZnO in a mixture of aqueous solutions of zinc acetate dihydrate (0.2 M) and sodium hydroxide as precursors, under continuous and vigorous stirring at 60 °C in a 3:1 (V:V) ethanol-water mixture for 15 min. The pH value was previously adjusted at 9.5. HC was added in a proportion of 0.01 wt% and the mixture was heated at 60 °C for 4 h. The resulting grey precipitate of HC@ZnO was filtrated, washed with water/ethanol to remove the unreacted sodium acetate and then dried overnight at 100 °C (Scheme 1). Further, 3-chloropropyltrimethoxysilane (ClPTES) was grafted on HC@ZnO using ethanol/water 3:1 as a solvent at 80 °C during 5 h (Scheme 2). The resulting HC@ZnO–ClPTES sample was washed, filtrated, dried overnight at 80 °C and then prone to chlorine substitution by diethanolamine (DEA) at 50 °C under inert atmosphere for 24 h (Scheme 3).

The final HC@ZnO–Si–$(CH_2)_3$–$N(CH_2–CH_2–OH)_2$ material obtained denoted as HC@ZnO–Si–$N(OH)_2$ was washed, filtrated and

Please cite this article as: J. Vieillard et al., Metal-inorganic-organic core–shell material as efficient matrices for $CO_2$ adsorption: Synthesis, properties and kinetic studies, Journal of the Taiwan Institute of Chemical Engineers (2018), https://doi.org/10.1016/j.jtice.2018.08.020

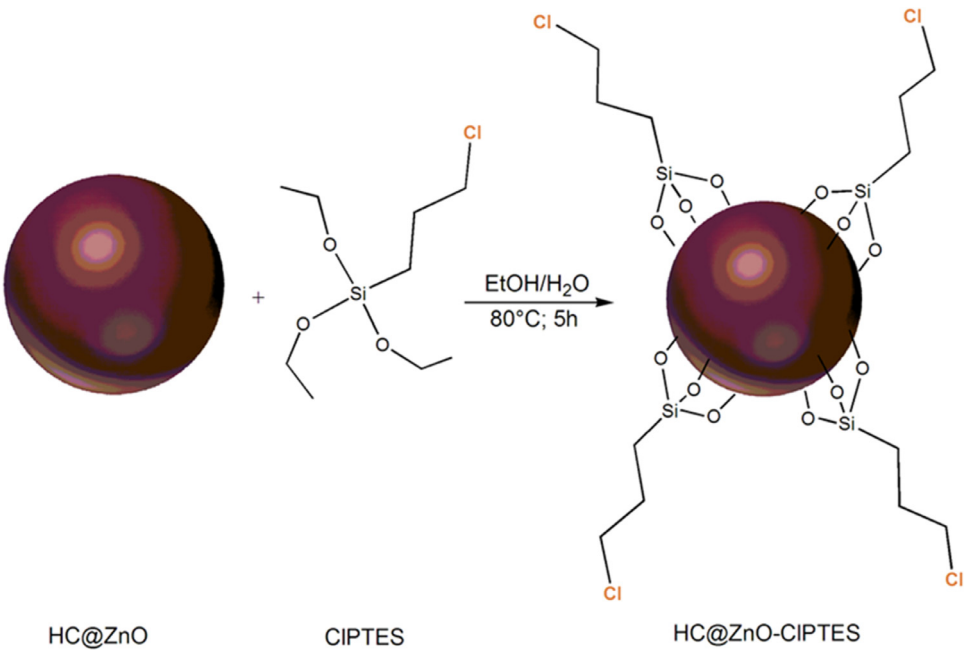


**Scheme 2.** Schematic illustration of the ClPTES grafting onto the surface of HC@ZnO.

then dried at 80 °C. Copper nanoparticles (CuNPs) were incorporated in HC@ZnO–Si–$N(OH)_2$ using 0.3 wt% anhydrous copper(II) sulfate ($CuSO_4$) as a precursor in 40 mL toluene in the presence of 0.03 wt% sodium borohydride ($NaBH_4$) as the metal reducing agent after 6 h of stirring at RT. The final HC@ZnO–Si–$N(OH)_2$–Cu material (Scheme 4), denoted as metal-inorganic-organic-core–shell (Cu-MIOCS) was dried overnight at 80 °C and then stored in sealed enclosure containing dried and $O_2$-free nitrogen.

### 2.3. Material characterization

HC, HC@ZnO and Cu-MIOCS were characterized through Fourier transform IR spectroscopy (FTIR) using a Tensor 27 (Bruker) spectrometer with a ZnSe ATR crystal equipment. For each spectrum, 20 scans were accumulated with a resolution of 4 $cm^{-1}$. All samples were drilled before IR analysis and background spectra were recorded on air. Analysis through Scanning Electronic Microscopy (SEM) of samples previously metallized by gold layer (at 18 mA during 360 s with a Biorad E5200 device) was performed by means of a ZEISS EVO 15 electron microscope. The surface morphology was investigated with secondary electrons, while the atomic composition was assessed by an attached Energy Dispersive X-ray Fluorescence (ED-XRF) device. The TEM (transmission electron microscopy) observations were achieved using a FEI TECNAI 20FST instrument on samples ultrasonically dispersed in ethanol and deposited on amorphous holey carbon membranes and then dried.

The specific surface area and porosity were assessed by nitrogen adsorption–desorption isotherms at 77 K, using a Micromeritics Tristar 3000 device. Typically, equivalent BET (Brunauer–Emmett–Teller) surface areas were determined in the relative pressure range P/P0 from 0.01 to 0.04 and equivalent BJH (Barrett–Joyner–Halenda) pore volume were measured at P/P0 > 0.985. The samples were previously degassed at 150 °C for at least 7 h using a Micromeritics Vac Prep 061 degasser. Measurements through differential scanning calorimetry (DSC) were carried out using (DSC-92 Setaram) at a 2 °C/min heating rate from room temperature to 500 °C. XPS analysis was performed using a Shimadzu ESCA-3400 and Al $K_{alpha}$ X-ray source (1486.6 eV), while deconvolution of the XPS patterns was achieved using a nonlinear least-square curve-fitting program (XPS-PEAK software 4.1). The zeta potential of each 2 mg of sample previously dispersed in 10 mL of deionized water and ultrasonicated for 15 min was measured with the phase analysis light scattering (PALS) mode using a Malvern zeta sizer nanoZS setup.

### 2.4. $CO_2$ adsorption tests and kinetics

This was achieved using an appropriate device containing dry air-free nitrogen according to a specific procedure fully described elsewhere [35]. Triplicate $CO_2$ adsorption tests were carried out within a 20 mL sealed enclosure at 292 K and normal pressure. Concisely, 3 mL of pure carbon dioxide previously dried was injected by a syringe in sealed capillary U-shaped manometer (0.25 mm internal diameter) containing dry air-free nitrogen and 0.01 g of dry material samples with a 2.43–5.14 µm particle size. The non-adsorbed $CO_2$ excess was further purged until the normal pressure is attained in the internal U-shaped manometer. The adsorbed $CO_2$ amount was periodically measured in time (0.2 min, 0.4 min, 0.6 min, 0.8 min, 1 min etc.) by measuring that of the residual non adsorbed gas. When necessary, complete regeneration for a total $CO_2$ release from the adsorbents was achieved by slight heating up to 80 °C or by forced convection under strong air stream (15–30 mL/min) until no $CO_2$ was detected by bubbling into a 0.1 N aqueous NaOH solution. The adsorbent affinity towards $CO_2$ was examined in terms of contact time and adsorption kinetics using pseudo 1st and 2nd order models [30,38,39].

## 3. Results and discussion

### 3.1. Surface morphology and textural properties

Same-scale SEM images (Fig. 1) (20 nm) revealed morphology change from fibrous HC (*a*) to granular HC@ZnO (*b*), suggesting strong HC: ZnO interaction. Much more pronounced changes were noticed after ClPTES (*c*) and diethanolamine grafting (*d*), resulting in aggregates of much smaller particles with particle size not exceeding few micrometers, presumably due to self-condensation of triethoxysilane groups and hydrophobic interaction between grafted chloro-propyl groups.

Please cite this article as: J. Vieillard et al., Metal-inorganic-organic core–shell material as efficient matrices for $CO_2$ adsorption: Synthesis, properties and kinetic studies, Journal of the Taiwan Institute of Chemical Engineers (2018), https://doi.org/10.1016/j.jtice.2018.08.020

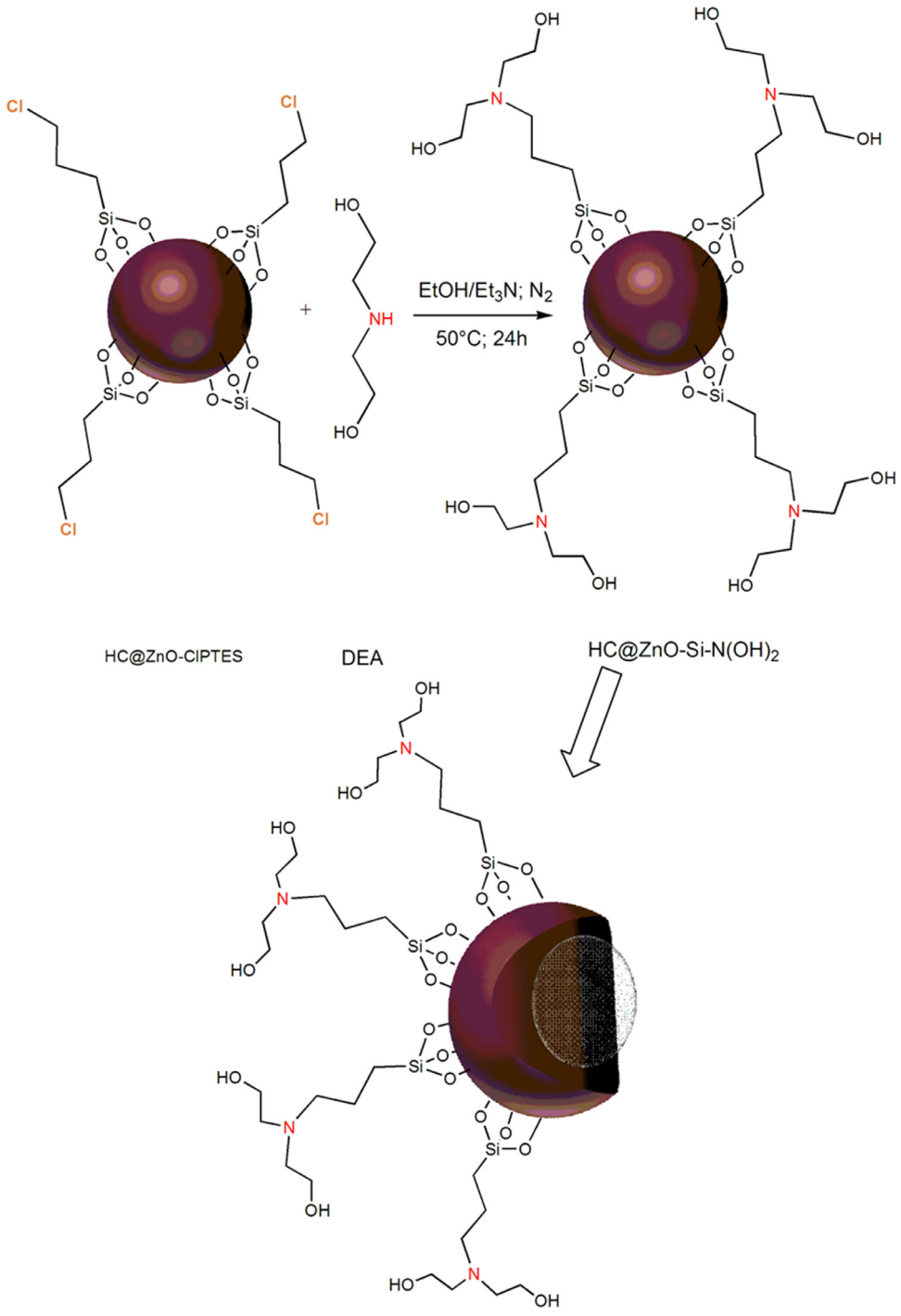


**Scheme 3.** Schematic illustration of the diethanolamine substitution of chloride on grafted ClPTES.

Further SEM images after $Cu^0$ incorporation (*e*) and close-up (*f*) showed larger aggregates of particles with much smoother external surface, most likely due intra and intergranular entrapment of $Cu^0$ particles. Here, strong $Cu^0$:$N(OH)_2$ Lewis-acid-base (LAB) interaction must induce a structure compaction that should reduce porosity, but should promote non-stoichiometric and purely physical condensation of $CO_2$ on metal sites surrounded by N atoms and hydroxyl groups.

Deeper insights through TEM images (Fig. 2) showed a clear membrane of ZnO shell surrounding aggregates of 0.05–0.1 µm dark stains of HC (*a*), whose aggregation generates interparticle void spaces (*a*). The latter appears to dramatically decrease upon ZnO-coating (*b*). After ClPTES grafting and further functionalization by diethanolamine (*c*), close-up on the clear membrane (*d*) and ED-XRF analysis revealed non uniformly sized 2–20 nm $Cu^0$ nanoparticles (CuNPs).

The nitrogen adsorption–desorption isotherms recorded were found to be of type IV with an H3-type hysteresis loop for mesoporous materials (Fig. 3). Measurements using the BET and BJH models (Table 1) revealed a structure expansion after ZnO incorporation as supported by the increase of the specific surface area (SSA) from 20 $m^2/g$ for HC to 25 $m^2/g$ for HC@ZnO.

The consecutive SSA decrease down to 21 $m^2/g$ upon ClPTES grafting agrees with our previous statement regarding a possible self-condensation of triethoxysilane groups and a structure compaction as a result hydrophobic interaction between grafted

Please cite this article as: J. Vieillard et al., Metal-inorganic-organic core–shell material as efficient matrices for $CO_2$ adsorption: Synthesis, properties and kinetic studies, Journal of the Taiwan Institute of Chemical Engineers (2018), https://doi.org/10.1016/j.jtice.2018.08.020

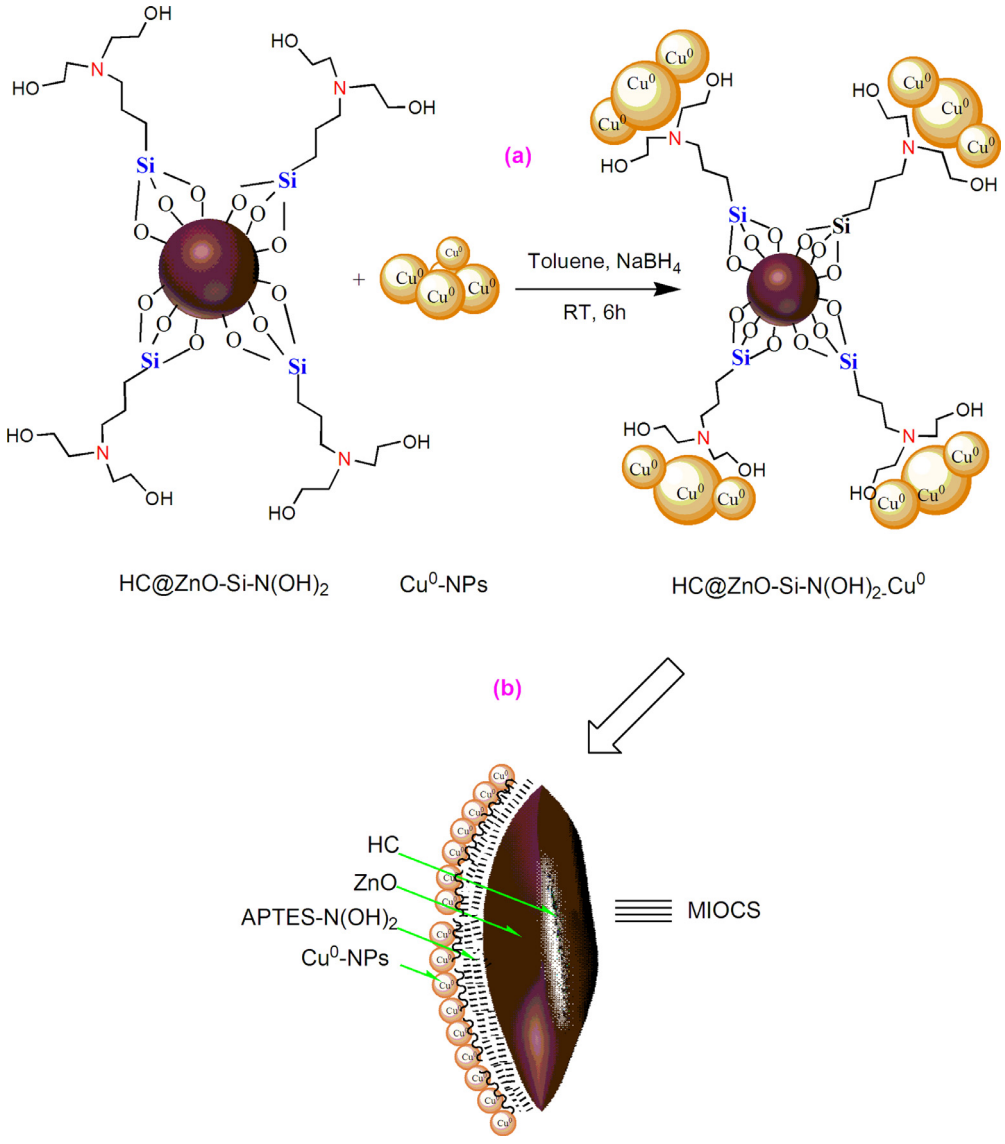


**Scheme 4.** Illustration of CuNPs insertion (a) and close-up on HC@ZnO–Si–$N(OH)_2$–Cu (b).

**Table 1**
Textural properties of the prepared samples.

| Sample | Isotherm | Hysteresis | Specific surface area ($m^2/g$) | Total pore volume (cc/g) | BJH pore volume (cc/g) |
|---|---|---|---|---|---|
| HC | – | – | 20 | – | – |
| HC@ZnO | Type II | H3 | 25 | 0.17 | 0.17 |
| HC@ZnO–ClPTES | Type II | H3 | 21 | 0.13 | 0.13 |
| HC@ZnO–Si–$N(OH)_2$ | Type II | H3 | 29 | 0.20 | 0.20 |
| Cu-MIOCS | Type II | H3 | 20 | 0.12 | 0.12 |

chloro-propyl groups. This is also supported by a porosity decay reflected by a pore volume decrease from 0.17 to 0.13 cc/g. Further functionalization with diethanolamine appears to suppress such an interaction, since a marked SSA improvement up to 29 $m^2/g$ was noticed. This must be due the appearance of H-bridges between terminal hydroxyls belonging to both the grafted organic moieties and residual free terminal Cu–OH groups. This is supposed to give rise to additional porosity, as supported by the significant increase in total pore volume from 0.12 to 0.20 cc/g.

$Cu^0$ particle insertion induced marked decay of the specific surface area and average pore volume down to 20 $m^2/g$ and 0.12 nm, respectively, thereby confirming our previously stated structure compaction. This phenomenon is a special feature of the occurrence of –N:Metal and -O:Metal Lewis-Acid-Base (LAB) interactions, as already reported elsewhere [14,36,40–43].

### 3.2. Evidence of metal stabilization

The most significant changes were noticed through FTIR analysis in the 750–1700 $cm^{-1}$ and 3000–3500 $cm^{-1}$ regions. These changes were mainly reflected by the rise of an intense absorption band at *ca.* 1065 $cm^{-1}$ and smaller one around 800 $cm^{-1}$ (Figs. 4, S1 and S2) attributed to Si–O–Si and Si–O–C stretching vibrations,

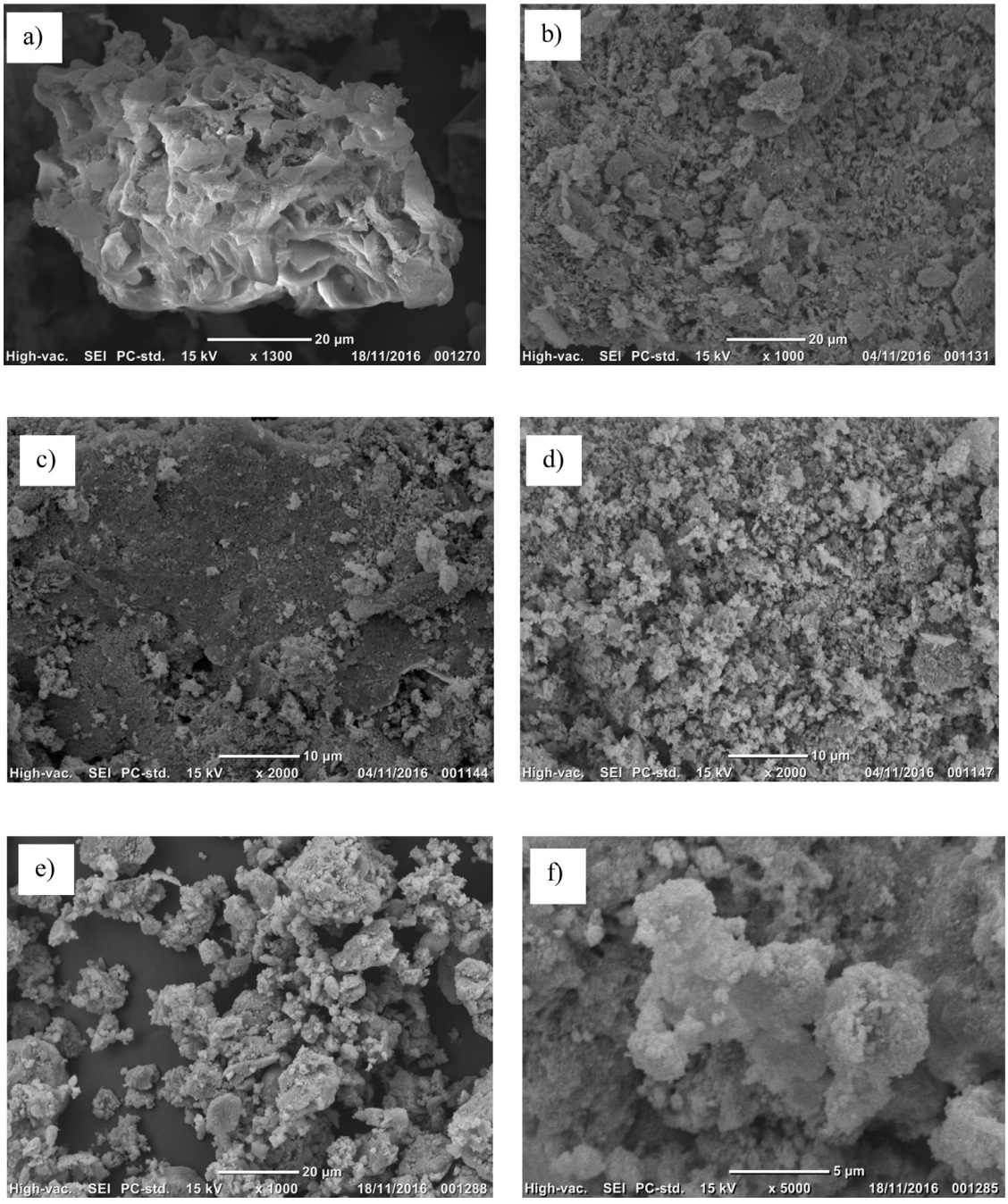


**Fig. 1.** SEM images of HC (a), HC@ZnO (b), HC@ZnO–ClPTES (c), HC@ZnO–Si–$N(OH)_2$ (d) and Cu-MIOCS (e and f).

providing clear evidence of ClPTES grafting but accompanied by an unavoidable self-condensation of the triethethoxysilane groups [35,44,45]. The appearance of the 3440–3700 and 1674 $cm^{-1}$ bands assigned to the N–H stretching vibration and $NH_2$ bending vibration, respectively was attributed to amine grafting [46,47]. The marked depletion of the 3400 $cm^{-1}$ after APTES grafting indicates the occurrence of HC–O–Si-propyl bridges.

The total disappearance of the 2919 $cm^{-1}$ band related to the asymmetric stretching vibration of $CH_2$ and C–H aliphatic groups after $Cu^0$ incorporation must be due to the occurrence of strong Cu: OH– and Cu:N– interactions that induce a compaction of the organic entanglement around CuNPs, in agreement with our previous statements [35,36]. Incorporation of CuNPs also induced a marked shift of the 1065 $cm^{-1}$ band towards lower wavenumber (Fig. 4), suggesting a N–C bond weakening by the appearance of strong $Cu^0$:N-propyl interaction. Terminal OH groups should also contribute to this compaction of the organic entanglement via $Cu^0$: OH- Lewis-acid-base interactions with a possible synergy between the N and O atoms in CuNP stabilization, as supported by the slight intensity decrease of the 3300–3600 $cm^{-1}$ bands [36,37].

Deeper insights through XPS analysis showed a shift of the O-1s signal from 529.98 eV to 530.53 peak after ClPTES grafting (Table 2). This can be explained in terms of a bond strengthening on the oxygen atom, most likely due to the genesis of Zn–O–Si and/or C–O–Si bridges. The O-1s binding energy values were in good agreement with those reported for ZnO [48]. Diethanolamine grafting induced a slight decrease of this binding energy from 530.53 eV to 530.42 eV, most likely due to the presence of high

Please cite this article as: J. Vieillard et al., Metal-inorganic-organic core–shell material as efficient matrices for $CO_2$ adsorption: Synthesis, properties and kinetic studies, Journal of the Taiwan Institute of Chemical Engineers (2018), https://doi.org/10.1016/j.jtice.2018.08.020

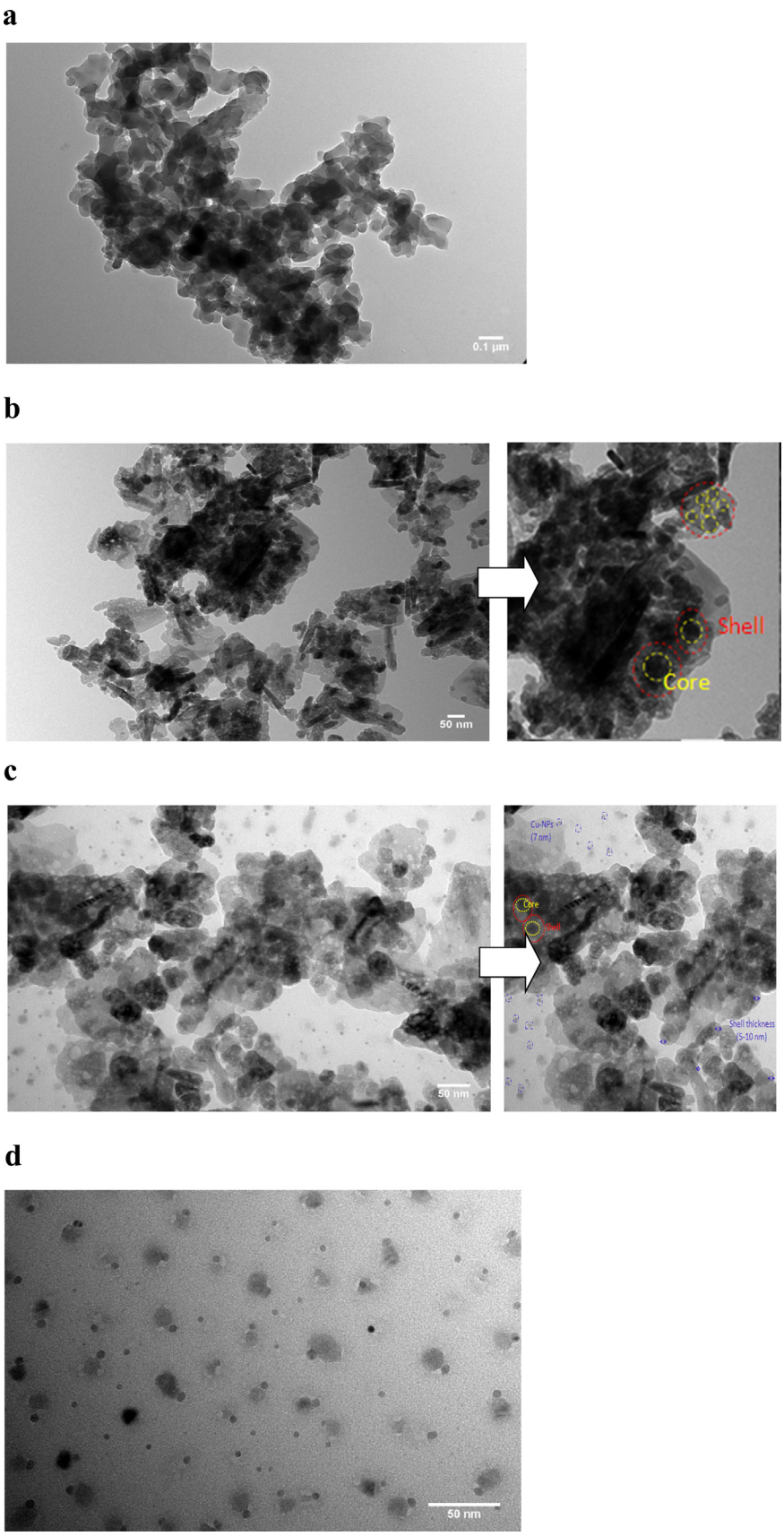


**Fig. 2.** TEM images of HC (a), HC@ZnO (b), Cu-MIOCS (c) and close-up on clear areas (d).

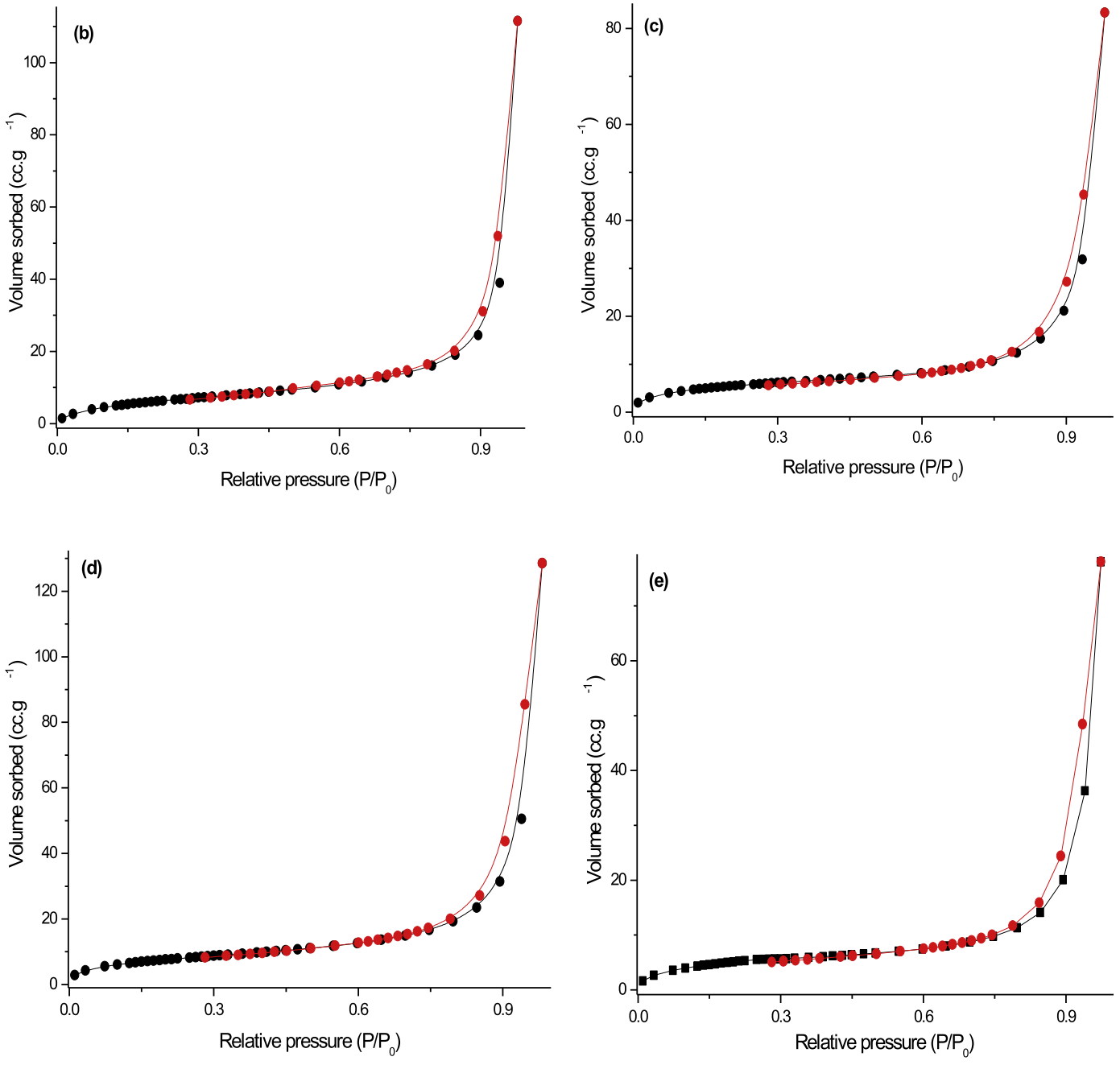


**Fig. 3.** Nitrogen adsorption–desorption of HC@ZnO (a), HC@ZnO–ClPTES (b), HC@ZnO–Si–$N(OH)_2$ (c) and Cu-MIOCS (d).

electron density due to next-neighboring N atoms. The involvement of the N and O atoms in CuNP stabilization was well supported by noticeable shifts of the binding energy of N-1s electrons from 399.71 to 400.33 eV and of O-1s electron from 530.42 eV to 530.91 eV, respectively, in agreement with previous data. [36] Cu incorporation was also supported by an additional Cu-2p signal at 935.70 eV (Table S1), with agrees with the literature [49].

HC encapsulation by ZnO was confirmed by the appearance of the Zn-$2p_{3/2}$ and Zn-$2p_{1/2}$ doublet at 1021.25 and 1044.34 eV, respectively [50]. The shift of both values up to 1022.24 and 1045.34 eV after ClPTES grafting accounts for a binding strengthening of the corresponding electrons, due to the formation of –Zn–O–Si–R bridges. These shifts indicate preponderant grafting of ClPTES on ZnO on HC [51]. The slight consecutive decrease of these values down to 1022.10 and 1045.30 eV must be due to the grafting of an electronegative atom (N). This was supported by the shift of the N-1s electron binding energy from 400.7 to 399.5 eV.

The C-1s XPS signal of HC@ZnO slightly shifted from 285.01 to 284.94, presumably as a result of an increase in electron density on ZnO by ClPTES grafting, which seems to act as "electron pump" due to the electronegativity of the chlorine atom. Chlorine substitution by diethanolamine grafting appears to revive the binding energy of the C-1s electrons, due to the higher electron density on the N atom. The fact that the binding energy of the C-1s electrons remained constant at 285.02 eV after $Cu^0$ incorporation indicates unequivocally that the organic chain grafted does not contribute to metal stabilization.

Metal stabilization was confirmed through additional Zeta potential measurements (Fig. 5), which revealed noticeable increases in the Zeta potential (ZP) and surface charge density (SPC) upon

Please cite this article as: J. Vieillard et al., Metal-inorganic-organic core–shell material as efficient matrices for $CO_2$ adsorption: Synthesis, properties and kinetic studies, Journal of the Taiwan Institute of Chemical Engineers (2018), https://doi.org/10.1016/j.jtice.2018.08.020

**Table 2**
Binding energies of the core level spectra for the different samples.

| Adsorbent | Binding energy (eV) | | | | | |
|---|---|---|---|---|---|---|
| | C-1s | O-1s | N-1s | Zn-2p$_{1/2}$ | Zn-2p$_{3/2}$ | Cu-2p |
| HC@ZnO | 285.01 | 529.98 | – | 1044.34 | 1021.25 | – |
| HC@ZnO–ClPTES | 284.94 | 530.53 | 400.07 | 1045.34 | 1022.24 | – |
| HC@ZnO–Si–N(OH)$_2$ | 285.02 | 530.42 | 399.71 | 1045.30 | 1022.10 | – |
| Cu-MIOCS | 285.02 | 530.91 | 400.33 | 1046.35 | 1023.19 | 934.70 |

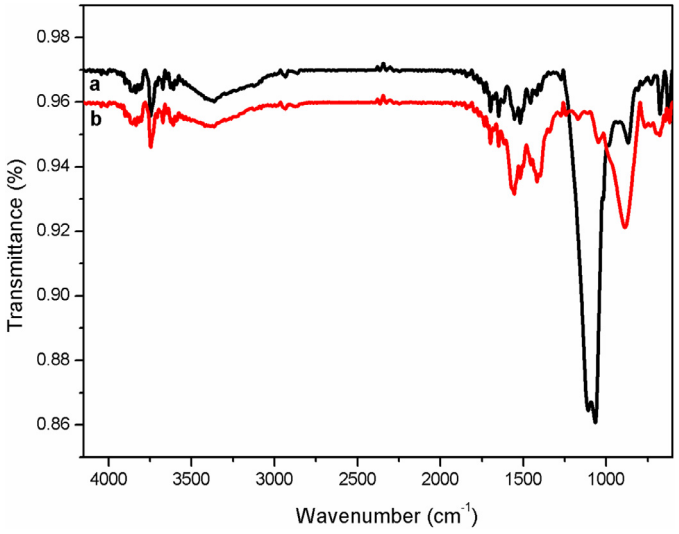


**Fig. 4.** FTIR spectra of HC@ZnO–Si–N(OH)$_2$ (a) and Cu-MIOCS (b).

ZnO incorporation. This must be due to the polarity of Zn–O bonds and terminal Zn–O–H groups [52]. Their consumption upon silylation by ClPTES induced a significant decrease of both the Zeta potential and surface charge density. Further functionalization by diethanolamine induced a slight SPC decrease but a marked ZP depletion.

Pronounced ZP depletion was registered after $Cu^0$ insertion, most likely due to the appearance of metal-matrice LAB interactions that favor the stability of the colloid suspension [53,54]. The fact that the zeta potential was reversed from positive to low negative value after $Cu^0$ incorporation must arise from an increase in electron density around CuNPs as a result of strong $Cu^0$: OH- and $Cu^0$–N- interactions.

### 3.3. Thermal behavior

DSC measurements (Fig. 6) showed thermal stability for HC up to 130–140 °C (*a*). Two exothermal processes were noticed around 250 °C and 450 °C due to the decomposition of cellulose and lignin, which are the main components of cocoa shell [55]. ZnO incorporation induced a stability improvement up to *ca.* 300 °C (*b*), as supported by the flattened bump around 350 °C. This can be explained by the formation of a more thermally stable inorganic ZnO shell.

HC@ZnO–Si–N(OH)$_2$ (*c*) displayed slightly lower thermal stability of up to 250 °C (*c*) due to the degradability of the grafted organic moiety. The latter appears to be enhanced by $Cu^0$ incorporation (*d*), presumably due to the appearance of copper-catalyzed decomposition processes.

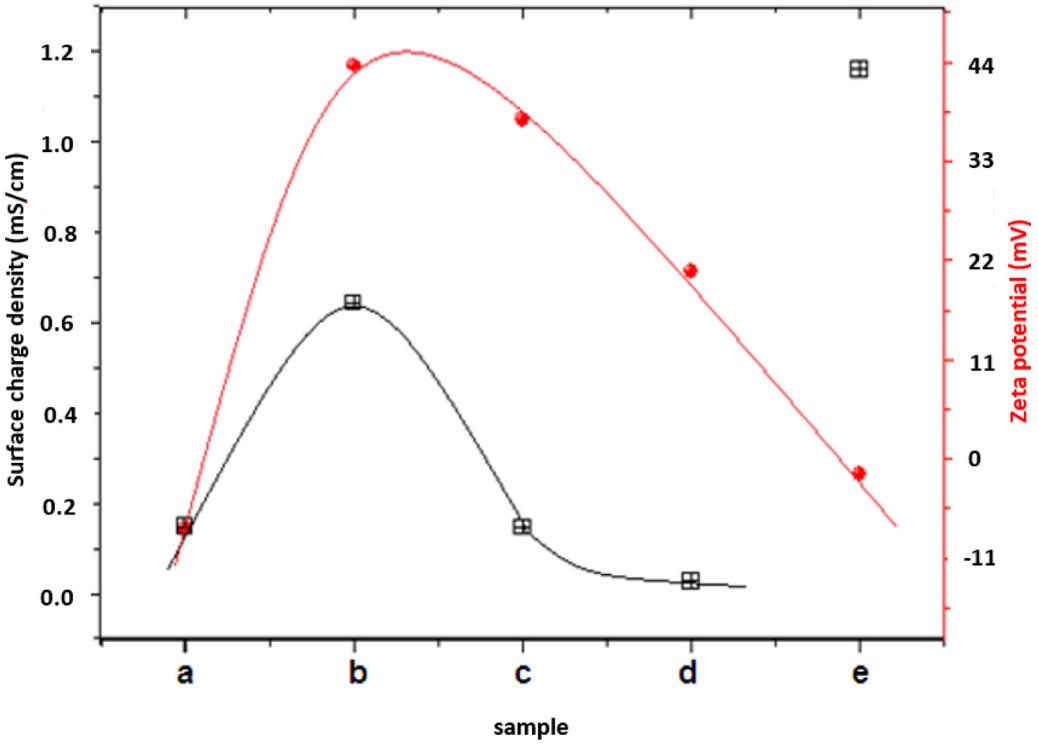


**Fig. 5.** Zeta potential (circle) and surface charge density (cross) for HC (a), HC@ZnO (b), HC@ZnO–ClPTES (c), HC@ZnO–Si–N(OH)$_2$ (d), and Cu-MIOCS (e).

Please cite this article as: J. Vieillard et al., Metal-inorganic-organic core–shell material as efficient matrices for $CO_2$ adsorption: Synthesis, properties and kinetic studies, Journal of the Taiwan Institute of Chemical Engineers (2018), https://doi.org/10.1016/j.jtice.2018.08.020

**Table 3**
Kinetics parameters for the intraparticle diffusion model.

| Sample | $k_{ID}$ [a] g/(mmol min$^{1/2}$) | $C_I$ [a] mmol/g | [c] $R^2$ | Standard deviation for $k_{ID}$ g/(mmol min$^{1/2}$) |
|---|---|---|---|---|
| HC | 0.43472 | 0.01087 | 0.934 | 0.05060 |
| HC@ZnO | 1.13768 | −0.00982 | 0.951 | 0.07745 |
| HC@ZnO–ClPTES | 1.34847 | −0.01047 | 0.977 | 0.06499 |
| HC@ZnO–Si–N(OH)$_2$ | 1.23477 | −0.06636 | 0.980 | 0.05337 |
| HC@ZnO–Si–N(OH)$_2$–Cu | 1.82982 | 0.26887 | 0.954 | 0.12614 |

[a] $k_{ID}$ is the constant for the intraparticle diffusion model.
[b] $C_I$ is assessed as the *Y*-axis intercept.
[c] $R^2$ is the correlation coefficient.

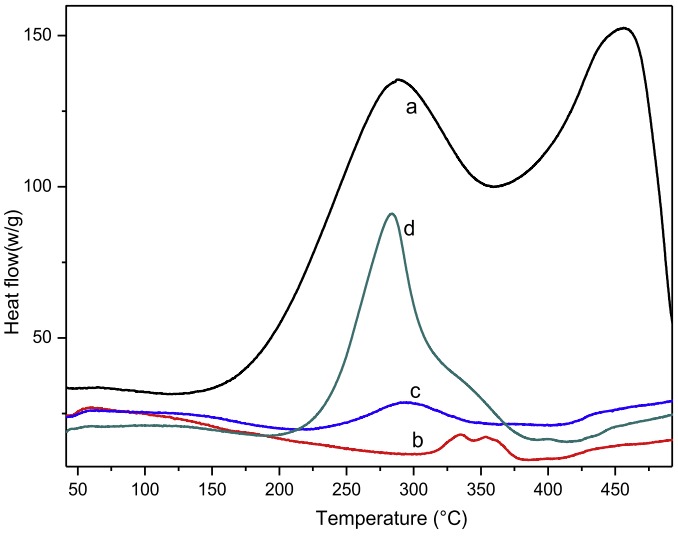


**Fig. 6.** DSC patterns of HC (a), HC@ZnO (b), HC@ZnO–Si–N(OH)$_2$ (c) and Cu-MIOCS (d).

### 3.4. Affinity towards $CO_2$ and adsorption kinetics

$CO_2$ adsorption tests under normal pressure and ambient temperature showed an increase in time of the amount of adsorbed $CO_2$ (Fig. 7). The latter reached a maximum and constant level after *ca.* 2 min for HC (*a*) and approximately 9–10 min for its modified counterparts (*b–d*).

It is worth mentioning that each material presents a reversible adsorption upon slight heating up 40 °C or under forced convection upon strong air stream of 15 mL/min with a maximum capacity for the first experiment. It results that, under these tests conditions, $CO_2$ adsorption must involve only weak interaction with the solid surface. This maximum level accounts for the real value of the $CO_2$ retention capacity (CRC) under these specific conditions. The highest $CO_2$ uptake was registered for Cu-MIOCS under normal pressure (5.423 mmol/g). This value is considerably higher than those registered under similar conditions for numerous other materials such as mesoporous silica [56], clays [12], zeolites [57], metal oxides [58], and others [56,59,60]. This improvement of the affinity towards $CO_2$ suggests simultaneous contributions of all incorporated species through specific interactions with a possible synergy that remains to be elucidated [61–65]. The slow evolution in time of the $CO_2$ uptake for the modified samples suggests the occurrence of diffusion hindrance. The two bump-shaped evolution curves suggest the occurrence of successive kinetic-determining steps, namely inter and intraparticle diffusion processes that differ from a sample to another according to the particle morphology and textural features [66].

Attempts to apply the pseudo 1st and 2nd order models [30,67] showed that $CO_2$ capture on HC obeys a pseudo-first order kinetics (Fig. 7). Here, physical adsorption through interactions between the oxygen atoms of carbon dioxide and terminal OH groups of HC seems to prevail in agreement with previous data [68–71] Nonetheless, neither models can apply to the other HC derivatives, the pseudo 1st order appearing as the most closest to the experimental curves. The most plausible explanation is that $CO_2$ adsorption on HC derivatives involves predominant kinetics-controlling diffusion processes and weak contributions of additional interaction involving both the amino and hydroxyl groups of the incorporated organic moiety [72] even in the presence of $Cu^0$ nanoparticles [16].

Deeper insights in $CO_2$ adsorption kinetics were achieved by applying the intraparticle diffusion (ID) model (Eq. (1)) that correlates the kinetics constant ($k_{ID}$) to the intraparticle diffusion constant (CI) [30]:

$$Q_t = k_{ID}.t^{1/2} + C_I \quad (1)$$

As expected, plotting $Q_t$ (instant $CO_2$ amount adsorbed) as a function of $t_{1/2}$ resulted in sufficiently linear correlations for almost all the synthesized samples, excluding HC (Fig. 8), thereby confirming the occurrence of intraparticle diffusion on HC derivatives.

The wide dispersion of the of the measured data gave estimated values of the correlation factor ($R^2$) ranging from 0.93 to 0.98 according to the sample texture, the closest to unity being those obtained for HC@ZnO–Si–N(OH)$_2$ (Table 3). In this adsorbent, the intraparticle diffusion appears to prevail more than in Cu-MIOCS, where other processes such as physical adsorption and multilayer $CO_2$ condensation should also take place at a more or lesser extent. The occurrence of different slopes accounts for that of different intraparticle diffusion constants within a same particle of a same adsorbent, in agreement with our previous statements and other works [73].

As expected, the values of $k_{ID}$ were found to vary in a reverse proportionality with the textural properties. Indeed, $k_{ID}$ increased from 1.13768 g/(mmol min$^{1/2}$) (HC@ZnO) to 1.34847 g/(mmol min$^{1/2}$) (HC@ZnO–ClPTES) and from 1.23477 g/(mmol min$^{1/2}$) (HC@ZnO–Si–N(OH)$_2$) to 1.82982 g/(mmol min$^{1/2}$) (Cu-MIOCS), when the total pore volume decreases from 0.17 to 0.13 cc/g and from 0.20 to 0.12 cc/g, respectively (Table 1). In the meantime the specific surface area decreases from 25 to 21 and from 29 to 20 m$^2$/g, respectively. This provides additional evidence of the enhancement of the diffusion contribution to the overall $CO_2$ retention process with the structure compaction. The mere fact that $CO_2$ desorbs only upon heating or forced convection clearly demonstrates the occurrence of effective physical $CO_2$ retention. The latter should probably occur in the form of multilayer condensation, more or less pronounced according to the pore size and surface affinity towards $CO_2$. Investigations are still in progress in this direction.

Please cite this article as: J. Vieillard et al., Metal-inorganic-organic core–shell material as efficient matrices for $CO_2$ adsorption: Synthesis, properties and kinetic studies, Journal of the Taiwan Institute of Chemical Engineers (2018), https://doi.org/10.1016/j.jtice.2018.08.020

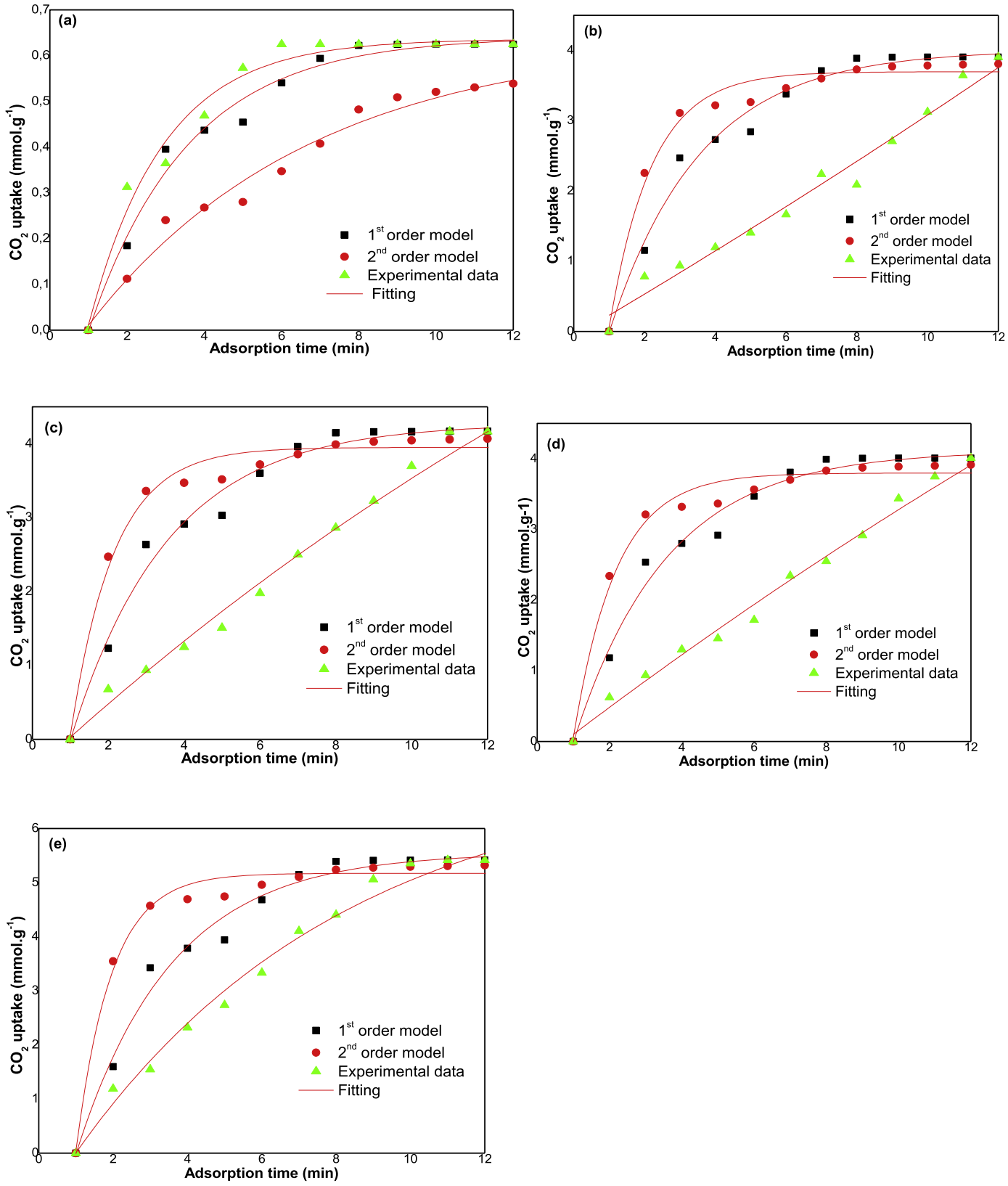


**Fig. 7.** Evolution in time of $CO_2$ uptake on hydrochar and modified derivatives as compared to adsorption kinetical models. (a) HC; (b) HC@ZnO; (c) HC@ZnO–ClPTES; (d) HC@ZnO–Si–$N(OH)_2$ and (e) Cu-MIOCS. These experiments were conducted by contacting, at room temperature and normal pressure, 10 mg of adsorbent previously dried overnight at room temperature with 3 mL of pure dry $CO_2$.

Please cite this article as: J. Vieillard et al., Metal-inorganic-organic core–shell material as efficient matrices for $CO_2$ adsorption: Synthesis, properties and kinetic studies, Journal of the Taiwan Institute of Chemical Engineers (2018), https://doi.org/10.1016/j.jtice.2018.08.020

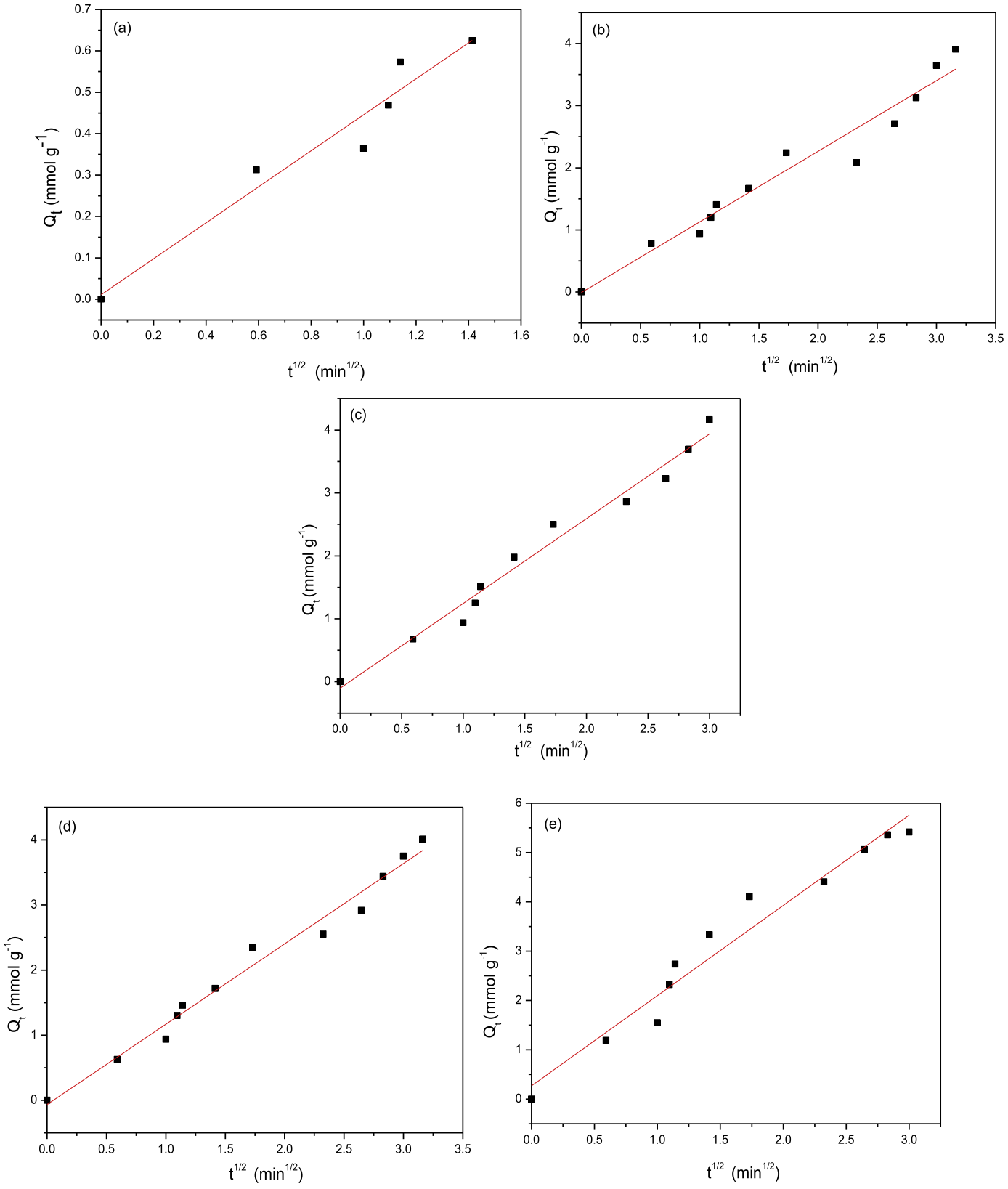


**Fig. 8.** Intraparticle diffusion model for $CO_2$ adsorption at ambient temperature and pressure of HC (a), HC@ZnO (b), HC@ZnO–ClPTES (c), HC@ZnO–Si–$N(OH)_2$ (d) and Cu-MIOCS (e).

Please cite this article as: J. Vieillard et al., Metal-inorganic-organic core–shell material as efficient matrices for $CO_2$ adsorption: Synthesis, properties and kinetic studies, Journal of the Taiwan Institute of Chemical Engineers (2018), https://doi.org/10.1016/j.jtice.2018.08.020

## 4. Conclusion

The present study provides the proof-of-concept that vegetal-deriving composites can display high affinity towards $CO_2$ at ambient temperature after judicious modification. Hydrochar encapsulation into HC@ZnO, functionalization with diethanolamino groups and copper incorporation produced an effective adsorbent for $CO_2$, affording an appreciable $CO_2$ uptake of 5.423 mmol/g. The latter was found to adsorb reversibly at ambient conditions, being easily released upon weak heating or forced convection. This was explained in terms of an attenuation of the Lewis basicity of the N atoms involved in $Cu^0$ stabilization and structure compaction. The appearance of –N:Metal and -O:Metal Lewis-Acid-Base (LAB) interactions are responsible of a structure compaction that promotes preponderantly physical interactions of $CO_2$ around entrapped CuNPs surrounded by O and N atoms belonging to the incorporated organic moiety. The easy $CO_2$ release only upon heating or forced convection must originate from effective physical adsorption of $CO_2$ in the form of multilayer condensation. This finding opens new prospects for the manufacture of highly added-value vegetal-deriving matrices for a reversible $CO_2$ capture. Significant affinity improvement towards $CO_2$ can be envisaged through judiciously tailored material texture and surface interaction. Investigations are still in progress in this direction.

## Author contributions

The manuscript was written through contributions of all authors. All authors have given approval to the final version of the manuscript.

## Acknowledgment

This work was partially supported by INSA Rouen, Rouen University, CNRS, Labex SynOrg (ANR-11-LABX-0029), the European Battuta Program, the European FEDER program, the Normandy region (CBS network) and the Evreux Portes de Normandie Agglomeration. We thank Dr. Philippe Decorse from ITODYS (UMR 7086 CNRS) for the XPS analysis.

## Supplementary materials

The TEM image of the distribution of Cu nanoparticles; XPS analysis and chemical composition for the different samples; $CO_2$ adsorption measurements; IR analysis of $CO_2$-saturated materials; Kinetic parameters of pseudo 1st and 2nd order models.

Supplementary material associated with this article can be found, in the online version, at doi:10.1016/j.jtice.2018.08.020.

## References

[1] Meinshausen M, Meinshausen N, Hare W, Raper SCB, Frieler K, Knutti R, et al. Greenhouse-gas emission targets for limiting global warming to 2 °C. Nature 2009;458:1158–62.
[2] MacDowell N, Florin N, Buchard A, Hallett J, Galindo A, Jackson G, et al. An overview of $CO_2$ capture technologies. Energy Environ Sci 2010;3:1645–69.
[3] Le Quéré C, Andrew RM, Canadell JG, Sitch S, Korsbakken JI, Peters GP, et al. Global carbon budget 2016. Earth System Sci Data 2016;8:605–49.
[4] Etheridge DM, Steele LP, Langenfelds RL, Francey RJ, Barnola JM, Morgan VI. Natural and anthropogenic changes in atmospheric $CO_2$ over the last 1000 years from air in Antarctic ice and firn. J Geophys Res: Atmos 1996;101:4115–28.
[5] Brunetti A, Scura F, Barbieri G, Drioli E. Membrane technologies for $CO_2$ separation. J Membr Sci 2010;359:115–25.
[6] Feng B, An H, Tan E. Screening of $CO_2$ adsorbing materials for zero emission power generation systems. Energy Fuels 2007;21:426–34.
[7] Rochelle GT. Amine scrubbing for $CO_2$ capture. Science 2009;325:1652.
[8] Sayari A, Belmabkhout Y. Stabilization of amine-containing $CO_2$ adsorbents: dramatic effect of water vapor. J Am Chem Soc 2010;132:6312–14.
[9] Veneman R, Zhao W, Li Z, Cai N, Brilman DWF. Adsorption of $CO_2$ and $H_2O$ on supported amine sorbents. Energy Procedia 2014;63:2336–45.
[10] Azzouz A, Assaad E, Ursu A-V, Sajin T, Nistor D, Roy R. Carbon dioxide retention over montmorillonite–dendrimer materials. Appl Clay Sci 2010;48:133–137.
[11] Azzouz A, Nousir S, Platon N, Ghomari K, Hersant G, Bergeron J-Y, et al. Preparation and characterization of hydrophilic organo-montmorillonites through incorporation of non-ionic polyglycerol dendrimers derived from soybean oil. Mater Res Bull 2013;48:3466–73.
[12] Azzouz A, Platon N, Nousir S, Ghomari K, Nistor D, Shiao TC, et al. OH-enriched organo-montmorillonites for potential applications in carbon dioxide separation and concentration. Sep Purif Technol 2013;108:181–8.
[13] Azzouz A, Ursu A-V, Nistor D, Sajin T, Assaad E, Roy R. TPD study of the reversible retention of carbon dioxide over montmorillonite intercalated with polyol dendrimers. Thermochim Acta 2009;496:45–9.
[14] Azzouz A, Nousir S, Bouazizi N, Roy R. Metal–inorganic–organic matrices as efficient sorbents for hydrogen storage. ChemSusChem 2015;8:800–3.
[15] Azzouz A, Aruş V-A, Platon N, Ghomari K, Nistor I-D, Shiao TC, et al. Polyol-modified layered double hydroxides with attenuated basicity for a truly reversible capture of $CO_2$. Adsorption 2013;19:909–18.
[16] Bouazizi N, Barrimo D, Nousir S, Ben Slama R, Roy R, Azzouz A. Montmorillonite-supported Pd0, Fe0, Cu0 and Ag0 nanoparticles: properties and affinity towards $CO_2$. Appl Surf Sci 2017;402:314–22.
[17] Nousir S, Platon N, Ghomari K, Sergentu AS, Shiao TC, Hersant G, et al. Correlation between the hydrophilic character and affinity towards carbon dioxide of montmorillonite-supported polyalcohols. J Colloid Interface Sci 2013;402:215–22.
[18] Choi S, Drese JH, Jones CW. Adsorbent materials for carbon dioxide capture from large anthropogenic point sources. ChemSusChem 2009;2:796–854.
[19] Sayari A, Belmabkhout Y, Serna-Guerrero R. Flue gas treatment via $CO_2$ adsorption. Chem Eng J 2011;171:760–74.
[20] Gassensmith JJ, Furukawa H, Smaldone RA, Forgan RS, Botros YY, Yaghi OM, et al. Strong and reversible binding of carbon dioxide in a green metal–organic framework. J Am Chem Soc 2011;133:15312–15.
[21] Gibson JAA, Mangano E, Shiko E, Greenaway AG, Gromov AV, Lozinska MM, et al. Adsorption materials and processes for carbon capture from gas-fired power plants: AMPGas. Ind Eng Chem Res 2016;55:3840–51.
[22] Sengupta S, Amte V, Dongara R, Das AK, Bhunia H, Bajpai PK. Effects of the adsorbent preparation method for $CO_2$ capture from flue gas using $K_2CO_3/Al_2O_3$ adsorbents. Energy Fuels 2015;29:287–97.
[23] Romero-Anaya AJ, Lillo-Ródenas MA, Linares-Solano A. Activation of a spherical carbon for toluene adsorption at low concentration. Carbon 2014;77:616–26.
[24] Heidari A, Younesi H, Rashidi A, Ghoreyshi AA. Evaluation of $CO_2$ adsorption with eucalyptus wood based activated carbon modified by ammonia solution through heat treatment. Chem Eng J 2014;254:503–13.
[25] Molina-Sabio M, Gonzalez MT, Rodriguez-Reinoso F, Sepúlveda-Escribano A. Effect of steam and carbon dioxide activation in the micropore size distribution of activated carbon. Carbon 1996;34:505–9.
[26] Wang H, Gao Q, Hu J. High hydrogen storage capacity of porous carbons prepared by using activated carbon. J Am Chem Soc 2009;131:7016–22.
[27] Rivera-Utrilla J, Sánchez-Polo M, Gómez-Serrano V, Álvarez PM, Alvim-Ferraz MCM, Dias JM. Activated carbon modifications to enhance its water treatment applications. An overview. J Hazard Mater 2011;187:1–23.
[28] Gęsikiewicz-Puchalska A, Zgrzebnicki M, Michalkiewicz B, Narkiewicz U, Morawski AW, Wrobel RJ. Improvement of $CO_2$ uptake of activated carbons by treatment with mineral acids. Chem Eng J 2017;309:159–71.
[29] Bouazizi N, Ajala F, Bettaibi A, Khelil M, Benghnia A, Bargougui R, et al. Metal-organo-zinc oxide materials: investigation on the structural, optical and electrical properties. J Alloys Compd 2016;656:146–53.
[30] Bouazizi N, Khelil M, Ajala F, Boudharaa T, Benghnia A, Lachheb H, et al. Molybdenum-loaded 1,5-diaminonaphthalene/ZnO materials with improved electrical properties and affinity towards hydrogen at ambient conditions. Int J Hydrogen Energy 2016;41:11232–41.
[31] Wang X, Summers CJ, Wang ZL. Large-scale hexagonal-patterned growth of aligned ZnO nanorods for nano-optoelectronics and nanosensor arrays. Nano Lett 2004;4:423–6.
[32] Ren J, Musyoka NM, Langmi HW, North BC, Mathe M, Kang X. Fabrication of core–shell MIL-101(Cr)@UiO-66(Zr) nanocrystals for hydrogen storage. Int J Hydrogen Energy 2014;39:14912–17.
[33] Kobayashi H, Yamauchi M, Kitagawa H, Kubota Y, Kato K, Takata M. Hydrogen absorption in the core/shell interface of Pd/Pt nanoparticles. J Am Chem Soc 2008;130:1818–19.
[34] Kobayashi H, Yamauchi M, Kitagawa H, Kubota Y, Kato K, Takata M. Atomic-level Pd−Pt alloying and largely enhanced hydrogen-storage capacity in bimetallic nanoparticles reconstructed from core/shell structure by a process of hydrogen absorption/desorption. J Am Chem Soc 2010;132:5576–7.
[35] Vieillard J, Bouazizi N, Bargougui R, Brun N, Fotsing Nkuigue P, Oliviero E, et al. Cocoa shell-deriving hydrochar modified through aminosilane grafting and cobalt particle dispersion as potential carbon dioxide adsorbent. Chem Eng J 2018;342:420–8.
[36] Arus AV, Tahir MN, Sennour R, Shiao TC, Sallam LM, Nistor ID, et al. Cu0 and Pd0 loaded organo-bentonites as sponge-like matrices for hydrogen reversible capture at ambient conditions. ChemistrySelect 2016;1:1452–61.

[37] Tahir MN, Sennour R, Arus VA, Sallam LM, Roy R, Azzouz A. Metal organoclays with compacted structure for truly physical capture of hydrogen. Appl Surf Sci 2017;398:116–24.
[38] Loganathan S, Tikmani M, Edubilli S, Mishra A, Ghoshal AK. $CO_2$ adsorption kinetics on mesoporous silica under wide range of pressure and temperature. Chem Eng J 2014;256:1–8.
[39] Ouargli-Saker R, Bouazizi N, Boukoussa B, Barrimo D, Paola-Nunes-Beltrao A, Azzouz A. Metal-loaded SBA-16-like silica – correlation between basicity and affinity towards hydrogen. Appl Surf Sci 2017;411:476–86.
[40] Bouazizi N, Barrimo D, Nousir S, Ben Slama R, Shiao TC, Roy R, et al. Metal-loaded polyol-montmorillonite with improved affinity towards hydrogen. J Energy Inst 2018;91:110–19.
[41] Bouazizi N, El achari A, Campagne C, Vieillard J, Azzouz A. Copper oxide coated polyester fabrics with enhanced catalytic properties towards the reduction of 4-nitrophenol. J Mater Sci: Mater Electron 2018;29:10802–13.
[42] Sennour R, Shiao TC, Arus VA, Tahir MN, Bouazizi N, Roy R, et al. Cu0-loaded organo-montmorillonite with improved affinity towards hydrogen: an insight into matrix-metal and non-contact hydrogen-metal interactions. Phys Chem Chem Phys 2017;19:29333–43.
[43] Tahir MN, Sennour R, Arus VA, Sallam LM, Roy R, Azzouz A. Metal organoclays with compacted structure for truly physical capture of hydrogen. Appl Surf Sci 2017;398:116–24.
[44] Sepehr MN, Kazemian H, Ghahramani E, Amrane A, Sivasankar V, Zarrabi M. Defluoridation of water via Light Weight Expanded Clay Aggregate (LECA): adsorbent characterization, competing ions, chemical regeneration, equilibrium and kinetic modeling. J Taiwan Inst Chem Eng 2014;45:1821–34.
[45] Yamaura M, Camilo RL, Sampaio LC, Macêdo MA, Nakamura M, Toma HE. Preparation and characterization of (3-aminopropyl)triethoxysilane-coated magnetite nanoparticles. J Magn Magn Mater 2004;279:210–17.
[46] Maurizi L, Claveau A, Hofmann H. Polymer Adsorption on iron oxide nanoparticles for one-step amino-functionalized silica encapsulation. J Nanomater 2015;2015:1–6.
[47] Saif B, Wang C, Chuan D, Shuang S. Synthesis and characterization of $Fe_3O_4$ coated on APTES as carriers for morin-anticancer drug. J Biomater Nanobiotechnol 2015;6:267–75.
[48] Figueiredo JL, Pereira MFR. The role of surface chemistry in catalysis with carbons. Catal Today 2010;150:2–7.
[49] Liu HL, Yang JH, Zhang YJ, Wang YX, Wei MB, Wang DD, et al. Ferromagnetism in Cu-doped ZnO nanoparticles at room temperature. J Mater Sci: Mater Electron 2009;20:628–31.
[50] Huang SY, Cheng QJ, Xu S, Wei DY, Zhou HP, Long JD, et al. Self-organized ZnO nanodot arrays: effective control using $SiN_x$ interlayers and low-temperature plasmas. J Appl Phys 2012;111:036101.
[51] Zhao L, Chen X, Wang X, Zhang Y, Wei W, Sun Y, et al. One-step solvothermal synthesis of a carbon@$TiO_2$ dyade structure effectively promoting visible-light photocatalysis. Adv Mater 2010;22:3317–21.
[52] Marsalek R. Particle size and zeta potential of ZnO. APCBEE Procedia 2014;9:13–17.
[53] Bhattacharjee S. DLS and zeta potential – what they are and what they are not? J Controlled Release 2016;235:337–51.
[54] Fritz G, Schädler V, Willenbacher N, Wagner NJ. Electrosteric stabilization of colloidal dispersions. Langmuir 2002;18:6381–90.
[55] Chen W-H, Kuo P-C. Isothermal torrefaction kinetics of hemicellulose, cellulose, lignin and xylan using thermogravimetric analysis. Energy 2011;36:6451–60.
[56] Sim K, Lee N, Kim J, Cho E-B, Gunathilake C, Jaroniec M. $CO_2$ adsorption on amine-functionalized periodic mesoporous benzenesilicas. ACS Appl Mater Interfaces 2015;7:6792–802.
[57] Yang S-T, Kim J, Ahn W-S. $CO_2$ adsorption over ion-exchanged zeolite beta with alkali and alkaline earth metal ions. Microporous Mesoporous Mater 2010;135:90–4.
[58] Ruminski AM, Jeon K-J, Urban JJ. Size-dependent $CO_2$ capture in chemically synthesized magnesium oxide nanocrystals. J Mater Chem 2011;21:11486–91.
[59] Sevilla M, Valle-Vigón P, Fuertes AB. N-doped polypyrrole-based porous carbons for $CO_2$ capture. Adv Funct Mater 2011;21:2781–7.
[60] Khalil SH, Aroua MK, Daud WMAW. Study on the improvement of the capacity of amine-impregnated commercial activated carbon beds for $CO_2$ adsorbing. Chem Eng J 2012;183:15–20.
[61] Hou X-J, He P, Li H, Wang X. Understanding the adsorption mechanism of $C_2H_2$, $CO_2$, and $CH_4$ in isostructural metal–organic frameworks with coordinatively unsaturated metal sites. J Phys Chem C 2013;117:2824–34.
[62] Tang Q-L, Luo Q-H. Adsorption of $CO_2$ at ZnO: a surface structure effect from DFT+U calculations. J Phys Chem C 2013;117:22954–66.
[63] Vinodh R, Bhagiyalakshmi M, Hemalatha P, Ganesh M, Peng MM, Palanichamy M, et al. Homopiperazine grafted mesoporous silicas from rice husk ash for $CO_2$ adsorption. J Nanosci Nanotechnol 2014;6:4639–48.
[64] Sneddon G, Greenaway A, Yiu HHP. The potential applications of nanoporous materials for the adsorption, separation, and catalytic conversion of carbon dioxide. Adv Energy Mater 2014;4:1301873. doi:10.1002/aenm.201301873.
[65] Yu C-H, Huang C-H, Tan C-S. A review of $CO_2$ capture by absorption and adsorption. Aerosol Air Qual Res 2012;12:745–69.
[66] Son W-J, Choi J-S, Ahn W-S. Adsorptive removal of carbon dioxide using polyethyleneimine-loaded mesoporous silica materials. Microporous Mesoporous Mater 2008;113:31–40.
[67] Ho Y-S. Review of second-order models for adsorption systems. J Hazard Mater 2006;136:681–9.
[68] Lu X, Jin D, Wei S, Zhang M, Zhu Q, Shi X, et al. Competitive adsorption of a binary $CO_2$–$CH_4$ mixture in nanoporous carbons: effects of edge-functionalization. Nanoscale 2015;7:1002–12.
[69] Jin D, Lu X, Zhang M, Wei S, Zhu Q, Shi X, et al. The adsorption behaviour of $CH_4$ on microporous carbons: effects of surface heterogeneity. Phys Chem Chem Phys 2014;16:11037–46.
[70] Wang Q, Zhang D, Wang H, Jiang W, Wu X, Yang J, et al. Influence of $CO_2$ exposure on high-pressure methane and $CO_2$ adsorption on various rank coals: implications for $CO_2$ sequestration in coal seams. Energy Fuels 2015;29:3785–95.
[71] Drage TC, Blackman JM, Pevida C, Snape CE. Evaluation of activated carbon adsorbents for $CO_2$ capture in gasification. Energy Fuels 2009;23:2790–6.
[72] Belmabkhout Y, Serna-Guerrero R, Sayari A. Adsorption of $CO_2$-containing gas mixtures over amine-bearing pore-expanded MCM-41 silica: application for gas purification. Ind Eng Chem Res 2010;49:359–65.
[73] Álvarez-Gutiérrez N, Gil M, Rubiera F, Pevida C. Kinetics of $CO_2$ adsorption on cherry stone-based carbons in $CO_2/CH_4$ separations. Chem Eng J 2017;307:249–57.

Please cite this article as: J. Vieillard et al., Metal-inorganic-organic core–shell material as efficient matrices for $CO_2$ adsorption: Synthesis, properties and kinetic studies, Journal of the Taiwan Institute of Chemical Engineers (2018), https://doi.org/10.1016/j.jtice.2018.08.020